CO_2 frost cap thickness on Mars during northern winter and spring

W. C. Feldman,[1] T. H. Prettyman,[1] W. V. Boynton,[2] J. R. Murphy,[3] S. Squyres,[4] S. Karunatillake,[4] S. Maurice,[5] R. L. Tokar,[1] G. W. McKinney,[1] D. K. Hamara,[2] N. Kelly,[2] and K. Kerry[2]

Received 10 April 2003; revised 14 June 2003; accepted 1 July 2003; published 4 September 2003.

[1] The thickness of seasonal CO_2 frost that covers the north pole of Mars during the winter and spring seasons is studied using gamma ray and neutron data measured using the gamma ray spectrometer suite of instruments aboard Mars Odyssey. The resultant seasonal variation of CO_2 ice/frost thickness for latitudes greater than +85° is in close agreement (within 9% at maximum) with those predicted using all three major Mars general circulation models presently in use. These observed CO_2 ice results are significantly different from those inferred from the Mars Obiter Laser Altimeter experiment aboard Mars Global Surveyor (MGS). A possible explanation is that the density of the CO_2 ice/frost cap is considerably lower than that inferred from observed variations of the MGS orbit. Other significant results are that the thermal neutron counting rates provide evidence for variations in the abundance of noncondensable components of the polar atmosphere of Mars and that the basement terrain below the seasonal cover of CO_2 frost within about 10° of the pole is nearly 100% water ice. *INDEX TERMS:* 6225 Planetology: Solar System Objects: Mars; 5462 Planetology: Solid Surface Planets: Polar regions; 5445 Planetology: Solid Surface Planets: Meteorology (3346); 5409 Planetology: Solid Surface Planets: Atmospheres—structure and dynamics; *KEYWORDS:* Mars, seasonal CO_2 frost cap, meteorology, polar regions, global circulation models

Citation: Feldman, W. C., et al., CO_2 frost cap thickness on Mars during northern winter and spring, *J. Geophys. Res.*, *108*(E9), 5103, doi:10.1029/2003JE002101, 2003.

1. Introduction

[2] Sensitive controlling factors of the Martian climate are the water and CO_2 frost deposits that have comprised the polar terrains of Mars intermittently throughout its history. During the present epoch, a large quantity of water ice persists throughout the year in the form of residual polar caps that cover both poles [*Thomas et al.*, 1992; *Carr*, 1996], as well as in the form of subsurface deposits poleward of about ±60° [*Boynton et al.*, 2002; *Feldman et al.*, 2002b; *Mitrofanov et al.*, 2002]. While the residual cap in the north consists of H_2O ice in direct contact with the atmosphere, the one in the south retains a perennial cover of CO_2 frost [*Kieffer*, 1979]. Superimposed seasonally on these materials are caps of CO_2 frost that precipitate or directly condense from the atmosphere during the local fall through spring portions of the year in each hemisphere. The thicknesses of these caps (geometric extent and column mass abundance) vary both with latitude and season. The advance and retreat of the seasonal cap margins are quite repeatable from year to year [*James and Cantor*, 2001]. However, relatively little is known about the spatial and time dependence of their thickness.

[3] Predictions of time variations of CO_2 frost thickness on a 7.5° latitude by 9° longitude grid have been made using the NASA Ames Research Center (ARC) Mars general circulation model (GCM) [*Pollack et al.*, 1990, 1993; *Haberle et al.*, 1993, 1999]. This model accounts for the full three-dimensional thermodynamics of the atmosphere (radiative heating, advection of heat and momentum, atmosphere-surface interaction, etc.) in addition to the condensation and sublimation of the predominant atmospheric gas, CO_2, when local vapor pressure exceeds the saturation vapor pressure. This model is in substantial agreement with two other GCMs [*Hourdin et al.*, 1995; *Richardson and Wilson*, 2002] through tuning all three to best fit the Viking observations. The possibility that Mars could experience such a condensation/sublimation of its main atmospheric component was first noted based upon results from a simple energy balance model [*Leighton and Murray*, 1966]. In that model, heat lost through radiation to the sky was balanced by latent heat of condensation, with heat advection parameterized as a tunable parameter. The GCM explicitly includes this heat advection term. Whenever and wherever CO_2 condensation occurs in the GCM, the condensed CO_2 is precipitated directly to the surface beneath its point of condensation.

[4] Seasonal variations of the zonally averaged geometric thickness of CO_2 frost in the northern hemisphere have previously been estimated using data from the Mars Orbiter Laser Altimeter (MOLA) on the Mars Global Surveyor (MGS) between 28 February 1999 and 25 May 2001 [*Smith*

[1]Los Alamos National Laboratory, Los Alamos, New Mexico, USA.
[2]Lunar and Planetary Laboratory, University of Arizona, Tucson, Arizona, USA.
[3]New Mexico State University, Las Cruces, New Mexico, USA.
[4]Cornell University, Ithaca, New York, USA.
[5]Observatoire Midi-Pyrenees, Toulouse, France.

0148-0227/03/2003JE002101

et al., 2001]. A complex pattern of frost buildup and decay was observed at latitudes poleward of about +65° N. Deposition began just after the autumnal equinox at an areocentric longitude of $L_S = 180°$. A series of dust storms interrupted this buildup temporarily between $215° < L_S < 270°$. Subsequent deposition produced a maximum physical thickness near the north pole at about $L_S = 345°$, followed by a slightly lower plateau that extended to about $L_S = 30°$, then to a minimum at about $L_S = 125°$. The magnitude of the maximum at +86.5° N latitude was 125 ± 25 cm, and the minimum at $L_S = 125°$ was about 30 ± 25 cm. A close study of the variations in spacecraft orbit in response to the redistribution of atmospheric mass onto and off the polar caps yielded an upper limit average CO_2 frost density of 0.91 ± 0.23 g cm^{-3}.

[5] In the present study, we extend our current knowledge of the northern seasonal CO_2 frost cap of Mars through use of gamma ray and neutron data measured using the gamma ray and neutron spectrometer components of the gamma ray spectrometer suite of instruments aboard the Mars Odyssey spacecraft. The quantity of measurement is the column mass of condensed CO_2 in g cm^{-2}. Measurements spanned the time interval just after insertion into mapping orbit on 18 February 2002 when $L_S = 329°$, through February 2003 when $L_S = 131°$. This initial analysis of GRS data will be limited to time-dependent variations in zonal (latitude) averages of the fluxes of the hydrogen 2.223 MeV gamma ray line and the thermal and epithermal neutrons. A study of the fast neutrons is reported separately (T. H. Prettyman et al., Composition and structure of the Martian surface in the high southern latitudes from neutron spectroscopy, submitted to *Journal of Geophysical Research,* 2003, hereinafter referred to as Prettyman et al., submitted manuscript, 2003), and that for a more complete analysis of the 2.223 MeV gamma ray line is given by N. J. Kelly et al. (Preliminary thickness measurements of the seasonal polar CO_2 frost on Mars, manuscript in preparation, 2003, hereinafter referred to as Kelly et al., manuscript in preparation, 2003). A determination of the thickness of the seasonal CO_2 frost deposit concentrates on subspacecraft positions poleward of +85° N latitude. These results are compared with those measured one Martian year earlier using MGS MOLA data, and with predictions made using the ARC GCM. These measured results provide another benchmark against which Martian atmospheric numerical models can be validated.

[6] A secondary goal of this study is to provide a 'ground truth' absolute normalization for the thermal and epithermal energy ranges of the Neutron Spectrometer to determine the composition of the residual polar cap beneath the seasonal CO_2 frost cap. It will be very important for determining the absolute abundance of hydrogen at all latitudes, which will be the subject of other studies.

2. Instrumentation

[7] The gamma ray spectrometer is a passively cooled, boom-mounted, 67 mm diameter by 67 mm long Ge crystal. Details of the instrumentation and general data reduction procedures are given separately [*Boynton et al.*, 2003]. The neutron spectrometer is a cubical block of borated plastic scintillator that is segmented into four prisms [*Feldman et al.*, 2002a; *Boynton et al.*, 2003]. The prism that is facing down to Mars (labeled P1) [see *Feldman et al.*, 2002a, Figure 1] is completely covered on the outside with Cd so that it responds only to epithermal and fast neutrons. Discrimination between the epithermal (approximately 0.4 eV to 700 keV) and fast (700 keV to about 2 MeV) energy ranges is made electronically [*Feldman et al.*, 2002a]. Thermal neutrons are separately measured by making use of the fact that the spacecraft travels faster (3.4 km/s) than a thermal neutron (1.9 km/s, corresponding to an average Martian temperature of about 220 K). The difference in counting rates between forward and backward facing prisms (labeled P2 and P4, respectively) is then used to subtract off the fraction of measured neutron fluxes that come from the spacecraft and the epithermal energy range. An overview of the technique and an explanation as to how it works is given in the literature [*Feldman and Drake*, 1986; *Feldman et al.*, 2002a; *Boynton et al.*, 2003].

3. Data Reduction and Analysis

[8] The temporal sampling interval of both neutron and gamma ray measurements is 19.75 s, which corresponds to a 1° arc of travel distance over the surface of Mars. Gamma ray spectra, as well as the counting rates of neutron fluxes in the three neutron energy ranges were summed separately for successive 5° latitude zones and about 7.5° areocentric longitude intervals. A sample of zonal averages of thermal and epithermal neutron counting rates, is shown in Figure 1. The traces for each L_S interval were forced to agree on average between ±40° latitude in order to correct for time variations in the thickness of the atmosphere, the cosmic ray intensity, and systematic uncertainties introduced in the numerical reduction procedure caused by changes in the high-voltage power supplies. The basis for this normalization is the known absence of extensive seasonally variable frost deposits at low latitudes on Mars.

[9] For the present study we concentrate on variations over the north polar cap (the south polar cap is studied separately (Prettyman et al., submitted manuscript, 2003)). Both the thermal and epithermal counting rate traces show generally similar behavior. At the earliest values of L_S that we studied, both rates decrease with increasing north latitude to a relative minimum at 60°–70° N before rising to a maximum at the north pole. With increasing L_S the depth of this relative minimum decreases monotonically, and its position shifts gradually northward. The polar maximum starts at mid range in our earliest L_S interval, rises to a maximum sometime after $L_S = 0°$, and then decreases to an absolute minimum at +87.5 N after $L_S = 100°$. Note that after $L_S = 100°$, the thermal trace shows a shallow minimum followed by a pronounced downward slope at about 77.5° N latitude. At this same latitude, the epithermal trace also shows an inflection in its downward slope of counting rate with increasing latitude at a given L_S.

[10] All the foregoing qualitative variations can be readily understood in terms of a spatially varying but temporally constant distribution of subsurface and surface water ice that is covered over by a CO_2 frost cap that varies in thickness with time and distance from the north pole. In order to

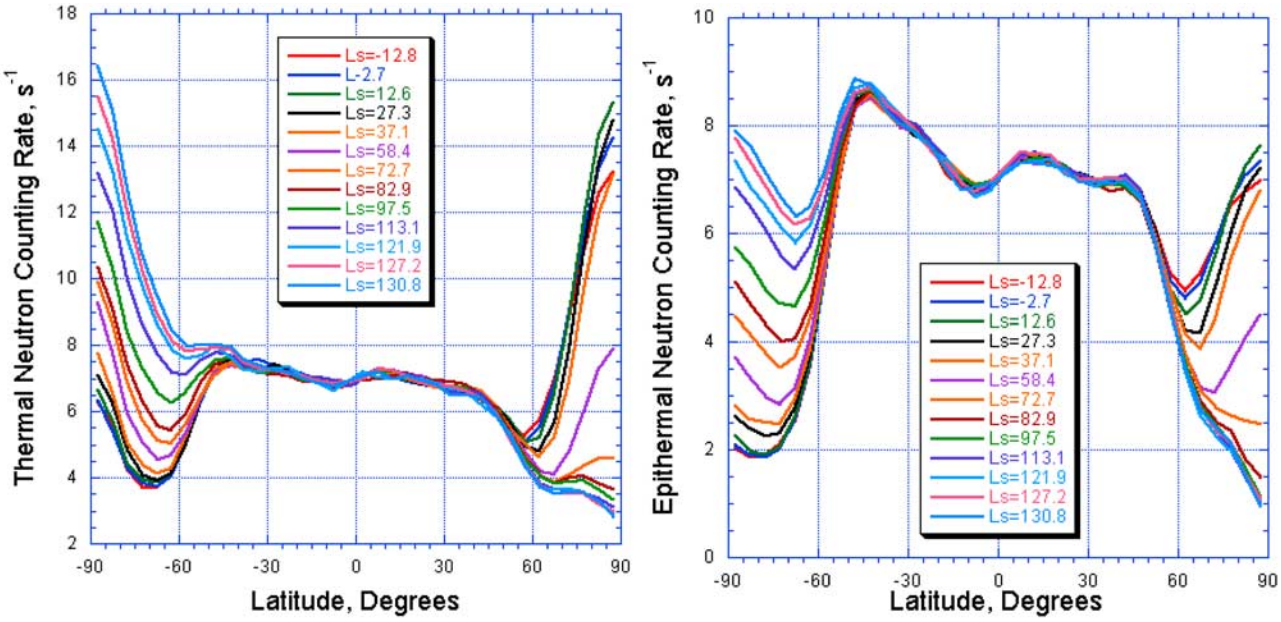

Figure 1. Zonal (latitude) averages of the (left) thermal and (right) epithermal neutron counting rates as a function of areocentric latitude L_S.

appreciate this fact, the results of several series of thermal and epithermal current simulations carried out using the Monte Carlo Neutral Particle code MCNPX (see, e.g., Prettyman et al., submitted manuscript, 2003, and references therein), are summarized in Figure 2. In all simulations, we assumed a semi-infinite basement deposit of soil having the elemental composition measured using the APXS experiment aboard Mars Pathfinder [*Wänke et al.*, 2001], mixed with varying weight percents of H_2O. Covering this basement is either a layer of pure CO_2 having varying thickness, or a layer of soil with varying thickness containing 1% and 2% H_2O (1% to 2% H_2O was chosen in accord with the analysis of reflectance IR observations made by *Houck et al.* [1973]). An atmosphere having the composition measured by Viking [*Owen et al.*, 1977] and a thickness of 20 g cm^{-2} (corresponding to a surface pressure of 744 Pascals) was used throughout.

[11] In this exercise, all simulated neutron spectra are fit by the published analytical model in their respective energy ranges, which consist of a superposition of thermal (α E exp[$-$E/E_o]) and epithermal (β E^{-p}) functions [*Drake et al.*, 1988; *Feldman et al.*, 2000]. The counting rates of the P1 (epithermal) and [P2$-$P4] (thermal) prism segments of the neutron spectrometer can then be related through integrals of the respective response function-weighted neutron currents simulated using MCNPX with input of a nominal isotropic cosmic ray energy distribution normalized to one proton cm^{-2} s^{-1}. Parameterizations of these simulated neutron flux distributions were given in the thermal (E < 0.4 eV) energy range by $Therm_m = \alpha E_o^2$, and in the epithermal energy range (0.4 eV < E < 0.7 MeV) by $Epi_m = \beta\ [E_2^{(1-p)} - E_1^{(1-p)}]/(1 - p)$ using E_1 = 1.56 eV and E_2 = 15.2 keV. This procedure was implemented using a set of 31 simulations chosen to span the full range of neutron flux functions used in Figure 2. A comparison of thermal and epithermal neutron counting rates with their respective parameterizations revealed very simple relations,

$$(P2 - P4) = \delta[0.081 + 16.8\ Therm_m]s^{-1} \quad (1)$$

$$P1 = \gamma\left[0.224 + 9.17\ Epi_m - 1.07\ Epi_m s^{-1}\right], \quad (2)$$

where $Therm_m$ and Epi_m are dimensionless numbers that are proportional to the upward thermal and epithermal neutron

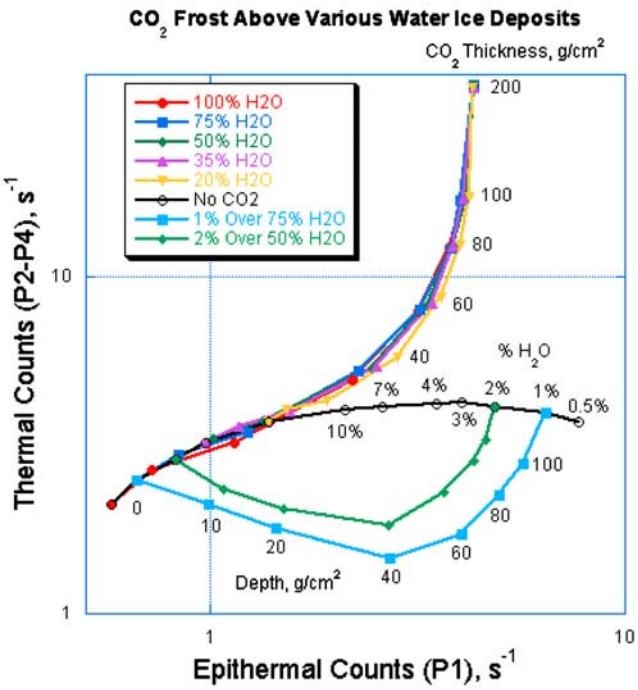

Figure 2. Simulated thermal and epithermal counting rates for selected models of polar terrains of Mars that span a large range of possible compositions. See text for details.

currents output by MCNPX. A simple quadratic model was found separately by Prettyman et al. (submitted manuscript, 2003) for fast neutron counting rates.

[12] The counting rates shown for thermal and epithermal neutrons in Figure 2 correspond to choosing $\delta = \gamma = 1$. Absolute values for δ and γ will be determined later in this study by comparing the sensor counting rates at the time of maximum CO_2 frost mass column abundance, to a set of simulations chosen to agree with the results of our determination of the thickness of the CO_2 frost cap at its maximum. An absolute normalization of fast neutron counting rates is determined by Prettyman et al. (submitted manuscript, 2003).

[13] An overview of all the simulations reveals that the different members of the series follow coherent patterns in the thermal-epithermal current space mapped in Figure 2. The simple semi-infinite soil composition series (given in black) shows a monotonic decrease in epithermal current with increasing water content, accompanied by first an increase in the thermal current to about 3% to 7% H_2O by weight, followed by a steady decline thereafter. The case of a semi-infinite layer containing 75% H_2O buried beneath a layer of varying thickness containing 1% H_2O is shown by the blue trace at the bottom. Note that it connects up with the black trace at 75% H_2O at zero thickness, and 1% H_2O at infinite thickness. A similar result that links 50% H_2O with 2% H_2O is shown by the green trace. Note that in both cases the thermal current reaches a minimum at between 30 and 40 g cm^{-2} overburden. We see that although not unique, the signature of buried water is a decreased current of thermal neutrons. The thermal current will also decrease in response to an enhanced abundance of neutron absorbing material such as Fe, Ti, Cl, N, Gd, and Sm [*Lingenfelter et al.*, 1961, 1972; *Feldman et al.*, 2000].

[14] The last series of runs involving layers of CO_2 frost above water-rich basement soils, all show behavior similar to one another. They connect up to the appropriate water-rich basement terrain at zero frost thickness (the black trace) and the thermal current increases monotonically with increasing CO_2 frost thickness. All traces begin to merge to a single trace beyond a thickness of about 40 g cm^{-2} because it becomes increasingly difficult to discriminate using neutron observations, the precise composition of the basement terrain when the overburden becomes thick. For thicknesses larger than about 80 to 100 g cm^{-2}, all traces become vertical, indicating a saturation of the epithermal neutron flux. Beyond this thickness, the water-rich basement terrain is no longer sensible in epithermal neutrons from orbit.

[15] We now return to the zonally averaged thermal and epithermal counting rate data shown in Figure 1. They show a modest cusp in the thermal rates and a downward inflection in the epithermal rates at about 77.5° latitude for L_S greater than about 100° when CO_2 frost is essentially absent. We see from the black, green, and blue lower traces in Figure 2 that this behavior is expected at the transition from subsurface water ice, found equatorward of about 77.5°, to the surface water ice of the permanent north polar cap.

4. Variations in Thickness of the CO_2 Frost Cap at the North Pole

[16] A comparison of three methods used to determine the time dependence of the column mass abundance of the CO_2 frost cap poleward of +85° N latitude is given in Figure 3. The most sensitive method to determine this thickness when it is low is to measure the attenuation of the gamma ray line at 2.223 MeV emitted by hydrogen contained within the underlying water ice-rich surface, as a function of L_S. The gamma ray line strength measured north of +85° latitude after all of the CO_2 has sublimed away (at about $L_S = 90°$) is then ratioed to the line strengths measured earlier. The time of complete disappearance of polar frost is verified by measuring a constant flux of 2.223 MeV gamma rays, as well as the currents of thermal and epithermal neutrons that are shown in Figure 4, after $L_S = 90°$. Attenuation of the 2.223 MeV gamma ray flux can be related to the thickness (in g cm^{-2}) of CO_2 overburden through the hydrogen gamma ray line strengths calculated in the series of simulations given by the upward red trace in Figure 2. This method therefore accounts for gamma ray attenuation and for the changing neutron environment brought about by the buildup of CO_2 frost (see Kelly et al. (manuscript in preparation, 2003) for more details). The results are given by the solid red circles in Figure 3. Earlier than $L_S = 35°$, the 2.223 MeV line strengths are so small that the correspondingly large uncertainty prevents any meaningful restriction on the CO_2 frost thickness, and so are not plotted.

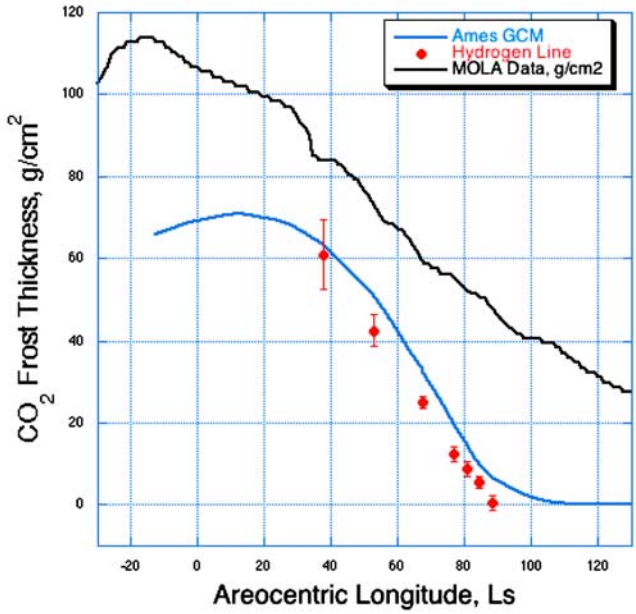

Figure 3. An overlay of three different measures of the seasonal variation of the CO_2 frost cap at the north pole of Mars. The GCM-predicted frost thickness is given by the blue curve, the CO_2 thickness inferred from measurements of the attenuation of 2.223 MeV gamma rays is given by the red circles, and the MOLA-derived thickness of CO_2 frost (given by column-integrated mass of CO_2 in g cm^{-2}) is given by the black line.

[17] For the purpose of this work, the ARC Mars GCM was run over an annual cycle with a fixed dust optical depth of 0.5. The ratio of visible-to-IR opacity was 2, consistent with observations [*Clancy et al.*, 1995]. The simulated annual pressure at the model's grid location nearest to that of the Viking Lander 1 location is within several tenths of a millibar

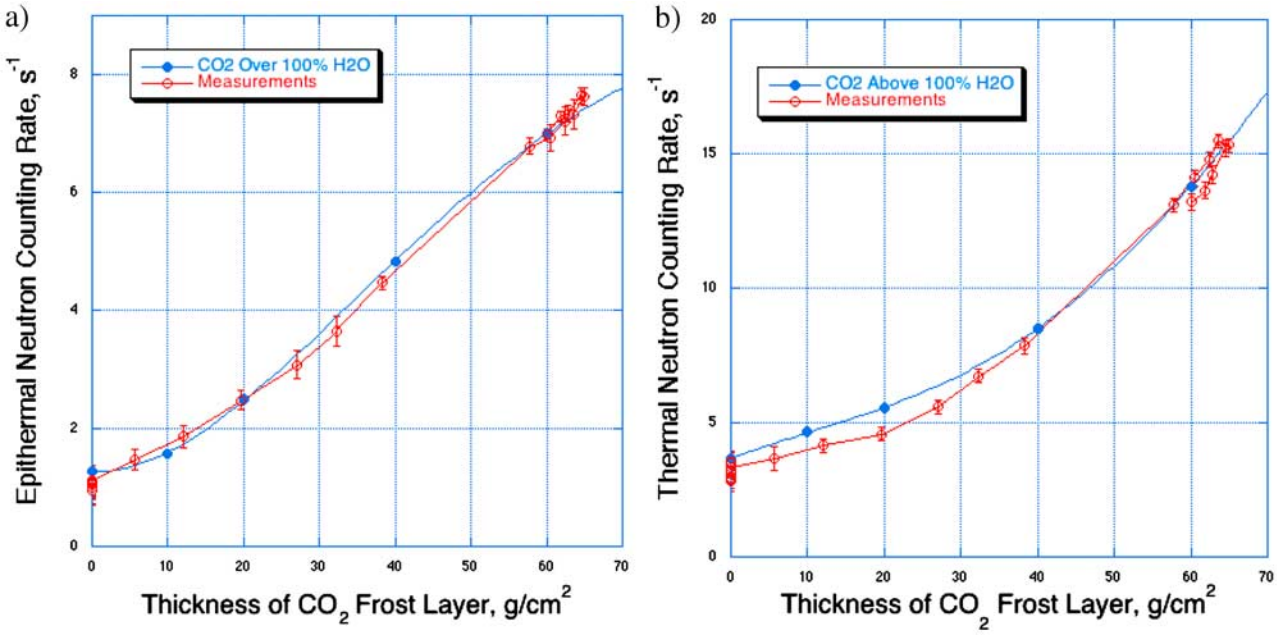

Figure 4. The measured (a) epithermal (red circles) and (b) thermal (red circles) counting rates as a function of the thickness of a CO_2 overburden. The blue lines (Figures 4a and 4b) give the simulated counting rates for models of a CO_2 frost layer of varying thickness above a basement terrain consisting of 100% H_2O. The line connecting the thermal neutron data points (Figure 4b) reveals the time ordering of the measurements (lower trace first followed by the upper trace).

to the observed cycle through the course of the simulated year, indicating that the model's CO_2 inventory is appropriate. Comparison of the gamma ray spectrometer inferred ice column abundance with the prediction of the ARC GCM simulation at 82.5° N latitude shows a close correspondence (a correlation coefficient of 0.99) with a constant offset of 6 ± 2 g cm^{-2}. The GCM-predicted frost thickness is given by the blue curve in Figure 3. The MOLA-derived CO_2 frost thickness (in g cm^{-2}) is given by the black line.

[18] In order both to check the assumption of a 100% water ice composition of the basement terrain used to convert the measured attenuation of the hydrogen gamma ray line to CO_2 frost thickness, and to provide an independent measure of the seasonal variation of CO_2 frost at the north pole, we compared the measured time variation of thermal and epithermal counting rates (given by the red circles in Figure 4) with those calculated using the MCNPX simulations (the blue curves in Figures 4a and 4b). The first step in this comparison is to determine the absolute normalization parameters, δ and γ, in equations (1) and (2), respectively. For this purpose, we choose the measured counting rates at the time when the corrected GCM-produced CO_2 frost thickness was near its maximum, greater than about 60 g cm^{-2}, because as shown in Figure 2, beyond a thickness of about 40 g cm^{-2} all simulations give the same thermal and epithermal counting rates regardless of the choice of basement terrain. This procedure gives, $\delta = 1.73 \pm 0.12$ and $\gamma = 2.2 \pm 0.11$. Use of these δ and γ multiplicative factors with the series of simulations in Figure 2 for a basement terrain composed of 100% H_2O, yields the blue lines in Figure 4.

[19] Inputs to our estimated uncertainties are derived from several sources added in quadrature. First, the dispersion between equations (1) and (2) with parameterizations of the sample of 31 neutron flux distributions simulated using MCNPX yields a root mean square percentage deviation of ±3% for the thermals and ±4% for the epithermals. Second, the standard deviations of the mean counting rates poleward of 85° N in eighteen 20° longitude intervals that circle the north pole when $15° < L_S < 20°$ yields the error bars shown in Figure 4 (which amount to approximately ±2% for both the thermal and epithermal counting rates for a CO_2 thickness greater than 50 g cm^{-2}). Last, the dispersion of counting rates measured when the thickness of CO_2 frost cover was greater than about 55 g cm^{-2} yields about ±3% for epithermal neutrons and ±6% for thermal neutrons. When combined in quadrature, the total uncertainty for δ normalization factor for thermal neutrons amounts to about ±7% and that for the γ normalization factor for epithermal neutrons is about ±5%.

[20] The fits between simulations for an assumed 100% H_2O residual cap below CO_2 frost of various thicknesses and the measurements are generally seen to be good. Although not shown here, a correspondingly good fit is obtained for the fast neutron counting rates (see Prettyman et al., submitted manuscript, 2003). Although the measured thermal counting rates fall a little below the simulated counting rates at intermediate CO_2 thicknesses, we conclude that the good agreement between all neutron and gamma ray observations analyzed with a model that uses GCM-predicted seasonal changes in the CO_2 frost thickness that cover a 100% water ice basement terrain, validates the Mars GCM.

5. Summary and Discussion

5.1. Time Dependence of the Seasonal CO_2 Polar Cap

[21] Thermal and epithermal neutron current intensities and the hydrogen capture gamma ray line strength at

2.223 MeV measured poleward of +85° N Latitude reveal the time variation of the column mass abundance of the north polar CO_2 frost cap during winter and spring. Gamma rays provide the most sensitive measure of this thickness when it is low, and epithermal neutrons are most sensitive when the thickness is high. Together, they validate the predictions of the ARC Mars GCM to within about 9% at maximum thickness.

[22] Comparison with the results determined from MOLA data measured one Martian year earlier [*Smith et al.*, 2001] reveals several interesting deviations. Not only does the MOLA-derived thickness reach a maximum earlier by about 25° in L_S, but its magnitude (assuming the upper limit density of 0.91 g cm^{-3}) is about 75% higher. Much of this discrepancy can be explained if the density of CO_2 frost was lower than the upper limit estimated by *Smith et al.* [2001]. This would not be surprising, since a bulk density of 0.91 g cm^{-3} would imply a porosity of 58%, and porosities substantially lower than this are not uncommon in freshly fallen snow or freshly condensed frost. In order to be consistent with our temporal trends in measured column mass abundances (which are in units of g cm^{-2}), the density would have to increase with time up to about L_S = 40°. This, too, is plausible, since both compaction and recrystallization can lead to densification of frost.

[23] However, time-dependent compaction of the CO_2 frost cannot explain why the MOLA thickness stays high relative to the Mars GCM prediction after L_S = 40° and never goes to zero during late northern spring/early northern summer. Indeed, the minimum cap thickness (during the season following cap sublimation) derived from MOLA data at +86.3° N never drops below about 30 ± 25 cm (at about L_S = 130°), which is not consistent with our results.

5.2. Nitrogen/Argon Abundance of the North Polar Atmosphere

[24] Another interesting observation can be made from the thermal and epithermal counting rates shown in Figure 4. Note that the epithermal counts are identical (within errors) for the increasing and decreasing time intervals of the cap frost thickness cycle (so too are the fast neutron counting rates (Prettyman et al., submitted manuscript, 2003)), while the thermal counts on the increasing portion of the cycle are systematically lower than those during cap sublimation. This thermal count effect can be explained if the column mass abundance of nitrogen and argon of the polar atmosphere is systematically higher when the frost cap is growing, and lower when it is declining. Such a result may be expected because both nitrogen and argon do not precipitate out of the atmosphere at the condensation temperature of the CO_2 frost cap and together have a relatively high thermal neutron absorption cross section. An enhanced column mass abundance of nitrogen and argon in the atmosphere at early times during the growth of the cap, should then act as a thermal neutron absorber, thereby decreasing the thermal neutron flux. At later times when the cap is subliming, thereby replenishing the atmosphere with pure CO_2, their combined abundance should decline, thereby producing a relative increase in the thermal neutron flux, as observed.

[25] The magnitude of this effect can be determined by comparing the thermal counting rates on the upper branch between 60 and 65 g cm^{-2} CO_2 thickness with those on the lower branch between 60 and 65 g cm^{-2} thickness, which yields a ratio of 1.08. This ratio in counting rates can be translated to effective variations in atmospheric weight fraction of (N_2 + A) through use of the MCNPX simulations shown in Figure 5. Shown here are neutron counting rates normalized to conditions of a standard atmosphere having 20 g cm^{-2} thickness and a 2.7% nitrogen weight fraction overlying a basement terrain consisting of 50 g cm^{-2} CO_2 frost overlying a semi-infinite layer of 100% H_2O. Argon was not included in this simulation because the cross section library that is available with our MCNPX code at Los Alamos does not include argon. However, the simulations shown in Figure 5 can be used nonetheless because we can define a nuclear effective nitrogen, N_{2eff}, that has the same total thermal absorption cross section as exhibited by 2.7% N_2 + 1.6% A. This procedure yields 3.3% N_{2eff}. We expect this simulation applies to conditions during the winter/spring season of the north polar cap of Mars because the ARC GCM predicts that the atmospheric thickness only varies between 18 and 22 g cm^{-2} during this period. Inspection shows that the epithermal and fast neutrons are insensitive to the N_2 weight fraction while the thermal neutron current decreases sharply with increasing N_2 weight fraction. This trend is qualitatively consistent with observations. Use of the quadratic fit to the thermal neutron rate calculations shown in Figure 5 gives a variation in N_{2eff} abundance that varies between 0.028 and 0.038 for the ±4% measured variation in thermal neutron counting rates. We note that this amplitude of variation is far smaller than

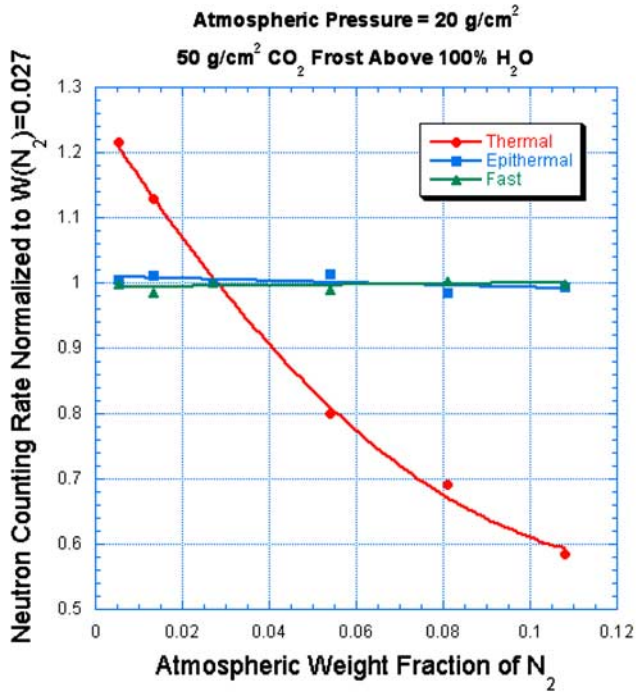

Figure 5. MCNPX simulations of neutron counting rates for a basement terrain composed of 50 g cm^{-2} CO_2 frost that covers a semi-infinite layer of 100% H_2O. A 20 g cm^{-2} atmosphere containing varying abundances of N_2 was assumed. All counting rates are normalized to unity at a weight fraction of 2.7% N_2.

would be expected if the atmosphere that freezes out onto the polar cap is replaced by more equatorial atmosphere that contains the average nitrogen plus argon abundance of N_{2eff} = 3.3% by weight. Because the polar atmosphere contains only about 20 g cm^{-2} and the maximum CO_2 frost thickness on the ground is 65 g cm^{-2}, about three atmospheres need to replace that frozen out. CO_2 condensation without horizontal mixing of the 'left behind' N_2 plus A gas would result in the polar atmosphere attaining N_{2eff} mass fractions of greater than 10%. That means that the composition of the final atmosphere could be a little more than a factor of four times more abundant in nitrogen plus argon than normal if indeed, the CO_2 portion of the atmosphere that condenses on the ground is replaced by atmosphere having a standard nitrogen plus argon abundance, and if no loss through lateral motion by eddy diffusion occurred.

[26] Obviously atmospheric dynamics must equalize the horizontal structure of atmosphere composition on the timescale of the northern Martian winter to restrain the build up of nitrogen plus argon abundance to only +15% and −18% relative to the normal 0.033 N_{2eff} atmospheric abundance. At least part of this restraint comes from the fact that the center of the north polar cap continues to accumulate CO_2 frost/ice long after the equatorial margins of the seasonal cap sublimes to replenish the polar atmosphere [*Haberle et al.*, 1979]. An important part of the replenished atmosphere that recondenses near the pole therefore contains no noncondensable gases.

5.3. Composition of the Basement Terrain Near the North Pole

[27] A final observation is that all the neutron data (thermal, epithermal, and fast currents) are fit using a model whose basal unit is a semi-infinite layer of nearly 100% water ice. Because about 36% of the footprint of the Neutron Spectrometer poleward of +85°N Latitude overlays layered terrain, this terrain must contain more than about a 75% weight fraction of H_2O to fit the data.

5.4. Model Validation

[28] Previously, model fidelity in regard to the annual CO_2 cycle has been judged based upon comparison between the Viking Lander pressure measurements and single-point model results at corresponding locations [*Wilson and Hamilton*, 1996; *Pollack et al.*, 1993]. However, as has been shown in the past, the local pressure is not simply representative of the global mean (appropriately scaled hydrostatically to 'sea level' or some other standard). A 'weather' signature is also present in the observed pressures [*Pollack et al.*, 1993; *Hourdin et al.*, 1995], with latitudinal surface pressure variations arising from latitude-dependent thermodynamic forcing. Our gamma ray and neutron spectrometer derived column ice abundances, when spatially integrated, provide a direct estimate of the amount of mass condensed from the atmosphere, which can be directly compared to spatial integration of the model results. Since this integrated effect is the result of the interplay between radiative and advective processes over an extended domain, small systematic local errors could accumulate to a large effect. Since both the local Viking Lander location comparisons and the larger-scale near-polar ice column abundance comparisons are both good, these results provide confidence in the model's ability to reproduce the global CO_2 cycle. Further work in extending the gamma ray and neutron spectrometer analysis to lower northern latitudes, and to the southern polar cap, will provide a stringent test of the model's ability to properly account for the Martian CO_2 cycle. The neutron spectrometer measurements are sensitive to both surface CO_2 (ice) as well as atmospheric CO_2 (vapor), and should be able to quantify the amounts of CO_2 in each of these reservoirs through the Martian year. We thus can anticipate obtaining an observationally derived quantification of the Martian CO_2 cycle against which models will be tested.

[29] **Acknowledgments.** We wish to thank many of the members of the GRS team for their criticisms and suggestions for clarifications at earlier stages of this study, and to the staff at U. of Arizona and JPL for their strong support of the ongoing operation of the instrument, the flow of data through the system, and the health of the spacecraft. We also wish to thank D. Smith and M. Zuber for help in interpreting the uncertainties of the MOLA measurements of the thickness of the northern CO_2 frost cap of Mars. Partial support of this work was provided by both the DOE (through laboratory directed research and development funds) and by NASA, and was conducted under the auspices of the DOE and the University of Arizona.

References

Boynton, W. V., et al., Distribution of hydrogen in the near surface of Mars: Evidence for subsurface ice deposits, *Science*, *2907*, 81–85, 2002.

Boynton, W. V., et al., The Mars Odyssey gamma-ray spectrometer instrument suite, *Space Sci. Rev*, in press, 2003.

Carr, M. H., *Water on Mars*, 229 pp., Oxford Univ. Press, New York, 1996.

Clancy, R. T., S. W. Lee, G. R. Gladstone, W. W. McMillan, and T. Rousch, A new model for Mars atmospheric dust based upon analysis of ultraviolet through infrared observations from Mariner-9, Viking, and Phobos, *J. Geophys. Res.*, *100*, 5251–5263, 1995.

Drake, D. M., W. C. Feldman, and B. M. Jakosky, Martian neutron leakage spectra, *J. Geophys. Res.*, *93*, 6353–6368, 1988.

Feldman, W. C., and D. M. Drake, A Doppler filter technique to measure the hydrogen content of planetary surfaces, *Nucl. Instrum. Methods Phys. Res., Sect. A*, *245*, 182–190, 1986.

Feldman, W. C., D. J. Lawrence, R. C. Elphic, D. T. Vaniman, D. R. Thomsen, B. L. Barraclough, S. Maurice, and A. B. Binder, Chemical information content of lunar thermal and epithermal neutrons, *J. Geophys. Res.*, *105*, 20,347–20,363, 2000.

Feldman, W. C., et al., Fast neutron flux spectrum aboard Mars Odyssey during cruise, *J. Geophys. Res.*, *107*(A6), 1083, doi:10.1029/2001JA000295, 2002a.

Feldman, W. C., et al., Global distribution of neutrons from Mars: Results from Mars Odyssey, *Science*, *297*, 75–78, 2002b.

Haberle, R. M., C. B. Leovy, and J. B. Pollack, A numerical model of the Martian polar cap winds, *Icarus*, *39*, 151–183, 1979.

Haberle, R. M., J. B. Pollack, J. R. Barnses, R. W. Zurek, C. B. Leovy, J. R. Murphy, H. Lee, and J. Schaeffer, Mars atmospheric dynamics as simulated by the NASA Ames General Circulation Model: 1. The zonal-mean circulation, *J. Geophys. Res.*, *98*, 3093–3124, 1993.

Haberle, R. M., M. M. Joshi, J. R. Murphy, J. R. Barnes, J. T. Schofield, G. Wilson, M. Lopez-Valverde, J. L. Hollingsworth, A. F. C. Bridger, and J. Schaeffer, General circulation model simulations of the Mars Pathfinder atmospheric structure investigation/meteorology data, *J. Geophys. Res.*, *104*, 8957–8974, 1999.

Houck, J. R., J. B. Pollack, C. Sagan, D. Schaack, and J. A. Decker, High altitude infrared spectroscopic evidence for bound water on Mars, *Icarus*, *18*, 470–480, 1973.

Hourdin, F., F. Forget, and O. Talagrand, The sensitivity of the Martian surface pressure to various parameters: A comparison between numerical simulations and Viking observations, *J. Geophys. Res.*, *100*, 5501–5523, 1995.

James, P. B., and B. A. Cantor, Martian north polar cap recession 2000 Mars orbiter camera observations, *Icarus*, *154*, 131–144, 2001.

Kieffer, H. H., Mars south polar spring and summer temperatures: A residual CO_2 frost, *J. Geophys. Res.*, *84*, 8263–8288, 1979.

Leighton, R. B., and B. C. Murray, Behavior of carbon dioxide and other volatiles on Mars, *Science*, *153*, 136–144, 1966.

Lingenfelter, R. E., E. H. Canfield, and W. N. Hess, The lunar neutron flux, *J. Geophys. Res.*, *66*, 2665–2671, 1961.

Lingenfelter, R. E., E. H. Canfield, and V. E. Hampel, The lunar neutron flux revisited, *Earth Planet. Sci. Lett.*, *16*, 355–369, 1972.

Mitrofanov, I., et al., Maps of subsurface hydrogen from the high energy neutron detector, Mars Odyssey, *Science*, *297*, 78–81, 2002.

Owen, T., K. Biemann, E. R. Rushneck, J. E. Biller, D. W. Howarth, and A. L. Lafleur, The composition of the atmosphere at the surface of Mars, *J. Geophys. Res.*, *82*, 4635–4639, 1977.

Pollack, J. B., R. M. Haberle, J. Schaeffer, and H. Lee, Simulations of the general circulation of the Martian atmosphere: 1. Polar processes, *J. Geophys. Res.*, *95*, 1447–1473, 1990.

Pollack, J. B., R. M. Haberle, J. Murphy, and H. Lee, Simulations of the general circulation of the Martian atmosphere: 2. Seasonal pressure variations, *J. Geophys. Res.*, *98*, 3125–3148, 1993.

Richardson, M. I., and R. J. Wilson, Investigation of the nature and stability of the Martian seasonal water cycle with a general circulation model, *J .Geophys. Res.*, *107*(E5), 5031, doi:10.1029/2001JE001536, 2002.

Smith, D. E., M. T. Zuber, and G. A. Neumann, Seasonal variations of snow depth on Mars, *Science*, *294*, 2141–2146, 2001.

Thomas, P., S. Squyres, K. Herkenhoff, A. Howard, and B. Murray, Polar deposits of Mars, in *Mars*, edited by H. H. Kieffer et al., pp. 767–795, Univ. of Ariz. Press, Tucson, 1992.

Wänke, H., J. Brückner, G. Dreibus, R. Rieder, and I. Ryabchikov, Chemical composition of rocks and soils at the pathfinder site, *Space Sci. Rev.*, *96*, 317–330, 2001.

Wilson, R. J., and K. Hamilton, Comprehensive model simulation of thermal tides in the Martian atmosphere, *J. Atmos. Sci.*, *53*, 1290–1326, 1996.

W. C. Feldman, G. W. McKinney, T. H. Prettyman, and R. L. Tokar, Los Alamos National Laboratory, Mail Stop D466, Los Alamos, NM 87545, USA. (wfeldman@lanl.gov)

W. V. Boynton, D. K. Hamara, N. Kelly, and K. Kerry, Lunar and Planetary Laboratory, University of Arizona, Tucson, AZ 85721, USA.

J. R. Murphy, Department of Astronomy, New Mexico State University, Las Cruces, NM 88001, USA.

S. Karunatillake and S. Squyres, Center for Radio-Physics and Space Research, Cornell University, Ithaca, NY 14853, USA.

S. Maurice, Observatoire Midi-Pyrenees, 31400 Toulouse, France.